© 2018. Published by The Company of Biologists Ltd | Journal of Cell Science (2018) 131, jcs212191. doi:10.1242/jcs.212191

RESEARCH ARTICLE

14-3-3 proteins regulate desmosomal adhesion via plakophilins

Katrin Rietscher, René Keil, Annemarie Jordan and Mechthild Hatzfeld*

ABSTRACT

Desmosomes are essential for strong intercellular adhesion and are abundant in tissues exposed to mechanical strain. At the same time, desmosomes need to be dynamic to allow for remodeling of epithelia during differentiation or wound healing. Phosphorylation of desmosomal plaque proteins appears to be essential for desmosome dynamics. However, the mechanisms of how context-dependent post-translational modifications regulate desmosome formation, dynamics or stability are incompletely understood. Here, we show that growth factor signaling regulates the phosphorylation-dependent association of plakophilins 1 and 3 (PKP1 and PKP3) with 14-3-3 protein isoforms, and uncover unique and partially antagonistic functions of members of the 14-3-3 family in the regulation of desmosomes. 14-3-3γ associated primarily with cytoplasmic PKP1 phosphorylated at S155 and destabilized intercellular cohesion of keratinocytes by reducing its incorporation into desmosomes. In contrast, 14-3-3σ (also known as stratifin, encoded by *SFN*) interacted preferentially with S285-phosphorylated PKP3 to promote its accumulation at tricellular contact sites, leading to stable desmosomes. Taken together, our study identifies a new layer of regulation of intercellular adhesion by 14-3-3 proteins.

KEY WORDS: 14-3-3 proteins, Desmosomes, Intercellular adhesion, Plakophilin

INTRODUCTION

Desmosomes are intercellular contacts that are essential for strong intercellular cohesion. They are especially abundant in tissues prone to mechanical strain, such as the skin and the heart. Cadherin function depends on the desmosomal plaque proteins plakoglobin (JUP) and plakophilins 1–3 (PKP1, PKP2 and PKP3), which act as scaffolds to link the desmosomal cadherins to desmoplakin (DSP). DSP in turn anchors keratin filaments. In the epidermis, the adhesive strength of desmosomes is controlled by PKP isoform expression. While PKP1 promotes the hyperadhesive state, to stabilize intercellular adhesion, PKP3 renders desmosomes more dynamic (Tucker et al., 2014; Keil et al., 2016). This facilitates tissue remodeling as required during regeneration and wound healing.

In addition, PKPs regulate cellular processes including protein synthesis, cell growth, proliferation and migration, and have been implicated in tumor development (Hatzfeld, 2007; Bass-Zubek et al., 2009; Kowalczyk and Green, 2013; Hatzfeld et al., 2014). PKP1 and PKP3 regulate the mRNA stability of specific targets including mRNAs encoding desmosomal proteins (Fischer-Keso et al., 2014). PKP1 controls cell proliferation and size by regulating protein synthesis via the translation initiation factor eIF4A1 (Wolf et al., 2010). This function is regulated by insulin/IGF-1 signaling via Akt2-mediated phosphorylation. Whereas un-phosphorylated PKP1 stabilizes cell adhesion in the desmosome, its phosphorylated form promotes proliferation in the cytoplasm and can induce anchorage-independent growth, a hallmark of cancer (Wolf et al., 2013). These studies support a context-dependent role for PKP1 in tissue regeneration and wound healing, as well as tumor formation.

14-3-3 proteins display widespread functions in diverse cellular processes including signal transduction, the cell cycle and apoptosis. They usually bind to phosphorylated serine/threonine (pS/T) residues, thereby influencing interactions of target proteins either by enabling or by blocking the access to other proteins (Aghazadeh and Papadopoulos, 2016). There are seven mammalian 14-3-3 family members, which occur as homo- or hetero-dimers. Each 14-3-3 molecule contains an independent ligand-binding site so that a dimer can bind two pS/T sites simultaneously, either on a single protein or on separate binding partners (Obsilova et al., 2014). Since 14-3-3 proteins have many partners that compete for binding, the affinity of partner proteins is an important factor in determining complex formation in the cell. The presence of more than one phosphosite can lead to a bidentate binding mode to the 14-3-3 dimer with dramatically enhanced affinity (Sluchanko, 2018). 14-3-3 proteins recognize pS/T residues in a sequence-specific context, and phosphorylation of these sites often depends on phosphoinositide 3-kinase (PI3K)/Akt signaling (Liu et al., 2002; Radhakrishnan and Martinez, 2010; Chen et al., 2011).

14-3-3σ (also known as stratifin, encoded by *SFN*) is highly expressed in the epidermis and its overexpression induces premature differentiation by suppressing IGF-1 signaling (Cianfarani et al., 2011). Inactivation of 14-3-3σ immortalizes keratinocytes (Dellambra et al., 2000), and epigenetic silencing of *SFN* has been reported in basal cell carcinoma supporting a tumor-repressive function (Lodygin and Hermeking, 2006). A heterozygous inactivating mutation of 14-3-3σ in mice causes the repeated epilation (Er) phenotype with hair loss and regrowth, and hyperproliferation of interfollicular epidermis, while homozygous *14-3-3σ-Er/Er* mice die at birth (Herron et al., 2005; Li et al., 2005; Sambandam et al., 2015). A 14-3-3σ–PKP3 association has been reported to limit PKP3 incorporation into desmosomes, although the physiological context regulating this interaction remains elusive (Roberts et al., 2013).

Based on the observation that 14-3-3γ-expressing fibroblasts grow in soft agar and form tumors in SCID mice, 14-3-3γ was considered to have an oncogenic potential. In agreement, 14-3-3γ is upregulated in various cancers (https://www.nextbio.com/). The oncogenic transformation mediated by 14-3-3γ depends on the activation of PI3K and MAPK signaling (Radhakrishnan and Martinez, 2010). On the other hand, 14-3-3γ has been reported to support cell–cell adhesion by facilitating the transport of desmosomal proteins to cell borders (Sehgal et al., 2014). How this function correlates with its overexpression in cancer remains to be elucidated.

Based on our recent finding on the regulation of PKP1 by PI3K/Akt signaling we asked whether Akt signaling generates 14-3-3 interaction sites within PKP1. Here we show that in mouse keratinocytes, 14-3-3σ

Institute of Molecular Medicine, Division of Pathobiochemistry, Martin-Luther-University Halle-Wittenberg, 06097 Halle, Germany.

*Author for correspondence (mechthild.hatzfeld@medizin.uni-halle.de)

M.H., 0000-0001-9968-7073

Received 20 December 2017; Accepted 11 April 2018

Journal of Cell Science (2018) 131, jcs212191. doi:10.1242/jcs.212191

and 14-3-3γ have opposing effects on desmosomal adhesion. 14-3-3γ destabilized desmosomes by re-localizing PKP1 to the cytoplasm whereas 14-3-3σ stabilized intercellular cohesion by targeting PKP3. Our data identify novel isoform-specific interactions between PKPs and 14-3-3 proteins that control desmosome stability.

RESULTS

14-3-3γ and 14-3-3σ are involved in keratinocyte adhesion

To assess which 14-3-3 isoform(s) contribute to the regulation of desmosomal adhesion in keratinocytes, we tested the expression of all seven 14-3-3 proteins. Because of considerable sequence conservation between the 14-3-3 proteins, we probed the specificity of isoform-specific 14-3-3 antibodies on recombinant 14-3-3 proteins. While most antibodies were specific, the anti-14-3-3η, -14-3-3β and -14-3-3ζ antibodies revealed some cross-reactions (Fig. S1). In the back skin of newborn mice and in spontaneously immortalized mouse keratinocytes 14-3-3γ, -σ, -ε and -η were highly expressed compared to the other isoforms (Fig. 1A,B). Given the abundance of desmosomal proteins in the skin, we assume that regulatory proteins that bind in a stoichiometric fashion occur at similar abundance. Therefore, we focused on the highly expressed isoforms 14-3-3γ, -σ, -ε and -η to analyze their contribution to keratinocyte cohesion. Dispase assays revealed that 14-3-3γ overexpression destabilized intercellular adhesion of mouse keratinocytes, whereas its knockdown did not interfere with strong intercellular cohesion. In contrast, 14-3-3σ overexpression was compatible with strong adhesion but its knockdown significantly reduced intercellular cohesion (Fig. 1C,D; see Fig. 5D,E for quantification). Neither 14-3-3γ nor 14-3-3σ knockdown affected the level of other 14-3-3 proteins (Fig. S2). 14-3-3ε and 14-3-3η did not reveal consistent effects on intercellular cohesion (data not shown). Taken together, these data suggest a destabilizing role of 14-3-3γ and a stabilizing role of 14-3-3σ in keratinocyte cohesion, in line with their reported roles in cancer.

14-3-3 proteins affect desmosomal protein localization

Since desmosomes mediate strong intercellular cohesion (Hatzfeld et al., 2017), we next asked whether 14-3-3 proteins regulate adhesion via desmosomal proteins. Therefore, we overexpressed 14-3-3 proteins in keratinocytes, and analyzed desmosomal proteins by immunofluorescence microscopy. 14-3-3γ induced a considerable decrease of junctional PKP1, whereas 14-3-3σ overexpression did not alter the distribution of PKP1 (Fig. 2A,B). In mouse keratinocytes, PKP3 accumulates at tricellular contact sites, whereas lateral (bicellular) contacts had a much weaker PKP3 association

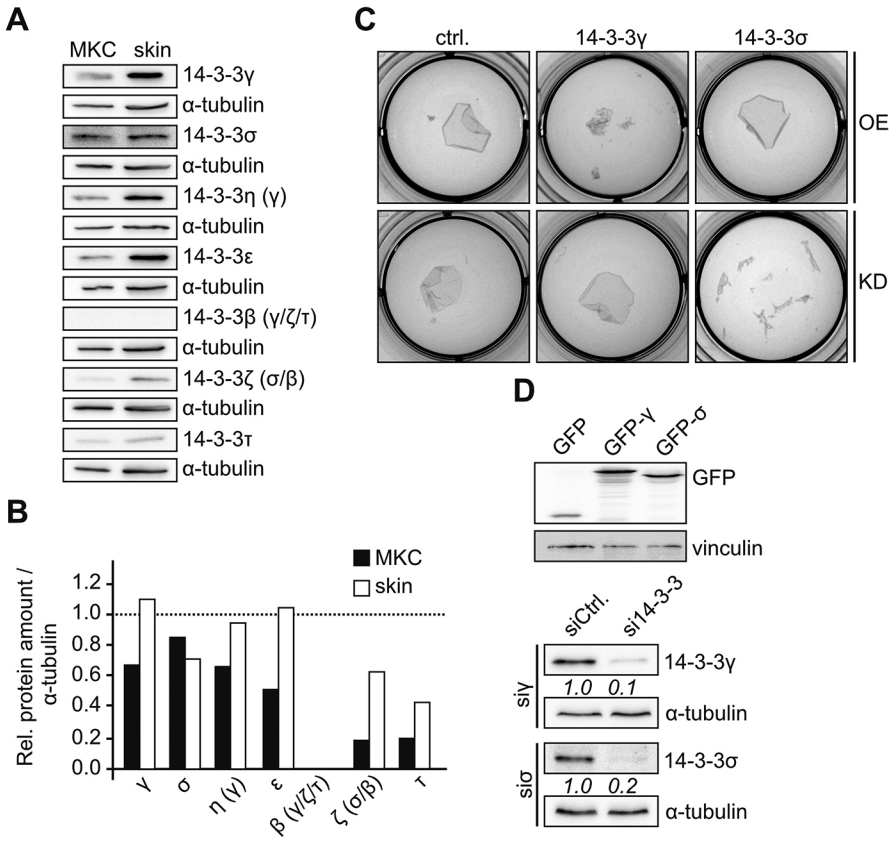

Fig. 1. 14-3-3γ and 14-3-3σ are highly expressed in murine skin and keratinocytes and have opposing effects on intercellular cohesion. (A) Western blot analysis of total protein extracts from mouse keratinocytes (MKC) grown for 6 days in HCM in comparison to extracts from newborn dorsal mouse skin. α-tubulin was used as loading control. Antibody cross reactivities for the 14-3-3 isoforms are indicated in brackets. (B) Quantification of 14-3-3 isoform amounts relative to α-tubulin in mouse keratinocytes (MKC) and dorsal skin of newborn mice. (C) Keratinocytes overexpressing GFP (ctrl.), GFP–14-3-3γ or GFP–14-3-3σ (overexpression, OE, upper row) or transfected with control, 14-3-3γ- or 14-3-3σ siRNAs (knockdown, KD, lower row) were cultured in HCM for 24 h. The monolayers were detached using dispase, subjected to mechanical stress for 60 min by orbital rotation at 300 rpm and documented using a digital camera. Representative pictures of epithelial sheets after application of mechanical stress are shown. The overexpression of 14-3-3γ and the knockdown of 14-3-3σ decreased epithelial sheet stability. (D) Fragments from experiments as in C (siγ, siRNA against 14-3-3γ; siσ, siRNA against 14-3-3σ) were collected by centrifugation, lysed in SDS sample buffer and processed for western blotting. Western blot analysis using an anti-GFP antibody confirmed overexpression of the indicated constructs. Vinculin was used as a loading control. Knockdown efficiencies were determined by western blotting with anti-14-3-3γ and anti-14-3-3σ antibodies, respectively. α-tubulin is shown as loading control. Knockdown efficiencies normalized to α-tubulin are given below the lanes.

Journal of Cell Science (2018) 131, jcs212191. doi:10.1242/jcs.212191

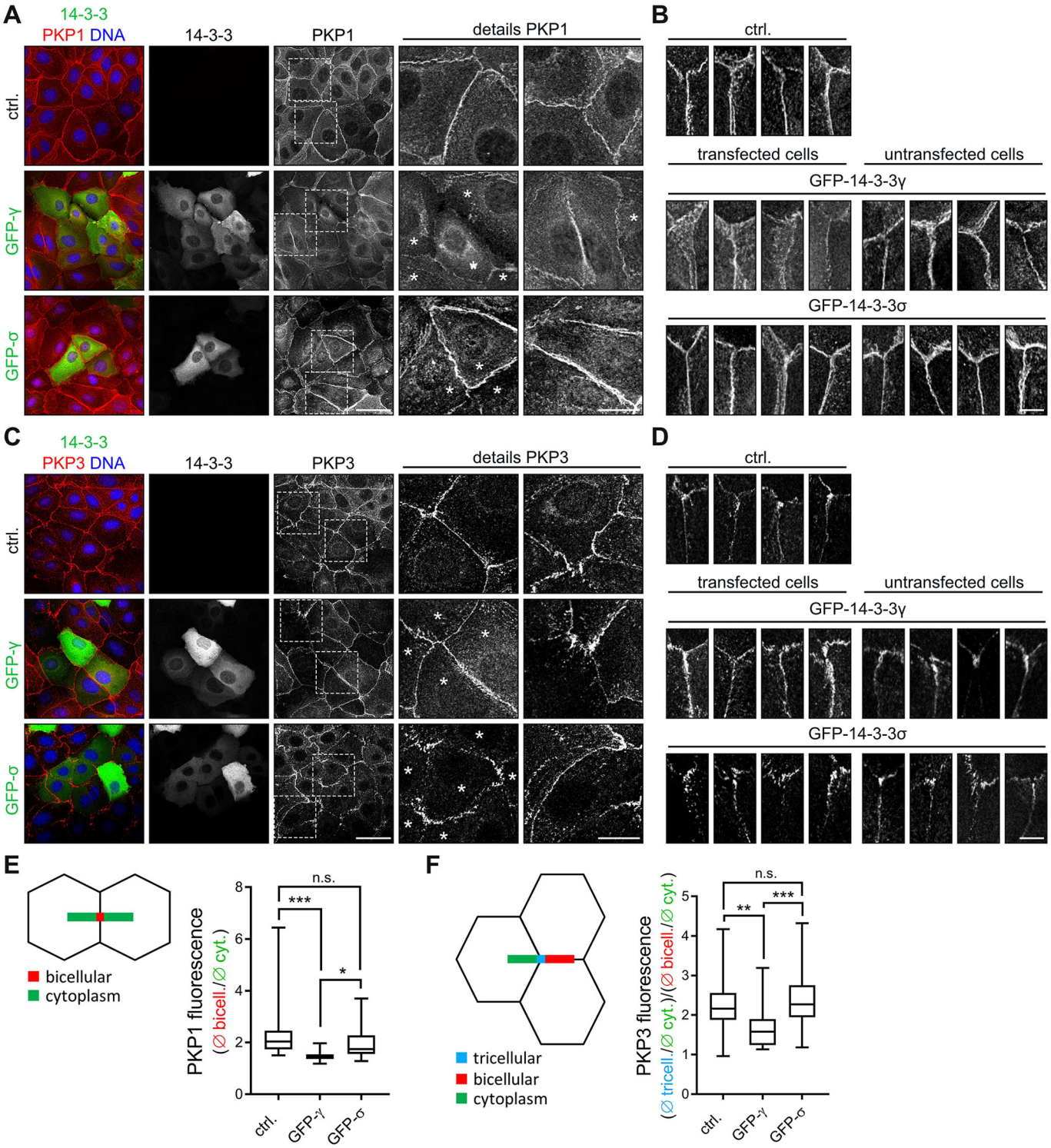

Fig. 2. 14-3-3γ and 14-3-3σ have opposing effects on the localization of PKP1 and PKP3 in mouse keratinocytes. Mouse keratinocytes transfected with the indicated GFP–14-3-3 constructs were grown for 24 h in HCM, fixed using MeOH at −20°C and immunostained for PKP1 (A,B) or PKP3 (C,D). Depicted are confocal images of single optical sections. Scale bars: 50 µm (main images), 10 µm (detail images). The enlargements highlight the differences between transfected (asterisks) and non-transfected cells. Galleries of PKP1 (B) and PKP3 (D) at bicellular and tricellular contacts emphasize the localization of PKP1 and PKP3 in 14-3-3γ- or 14-3-3σ-expressing cells compared to non-transfected cells from the same slide. Scale bar: 6.6 µm. 14-3-3γ-overexpressing cells exhibited a remarkable loss of junctional PKP1 compared to non-transfected cells, whereas PKP3 localization was increased at lateral compared to tricellular contacts after 14-3-3γ overexpression. 14-3-3σ overexpression did not significantly alter the localization of either PKP1 or PKP3, and was compatible with PKP3 accumulation at tricellular contacts. For quantification, PKP1 (E) and PKP3 (F) fluorescence intensities were determined using ImageJ by measuring segments of equal length and width across 30 individual bicellular or tricellular contacts as illustrated by the colored bars in the schematics. For each line scan, the mean junctional (bicellular, red; tricellular, blue) value was normalized to the mean cytoplasmic value (green). The boxplots (whiskers represent the range) depict the enrichment factor of PKP1 at bicellular (lateral) contacts or the ratio of PKP3 at tricellular versus bicellular contacts. **P*<0.05; ***P*<0.005; ****P*<0.0001; n.s., not significant (one-way ANOVA with Tukey's multiple comparisons test).

Journal of Cell Science (2018) 131, jcs212191. doi:10.1242/jcs.212191

(Keil et al., 2016). This distribution was changed upon 14-3-3γ overexpression, which induced an increased association of PKP3 with lateral contacts. Again, no changes were observed after 14-3-3σ overexpression (Fig. 2C,D). In order to quantify these findings we determined PKP1 fluorescence intensities across 30 bicellular (lateral) contacts as depicted in the scheme (Fig. 2E). These line scans were used to calculate the ratio of PKP1 at bicellular (lateral) contacts to cytoplasmic PKP1 as demonstrated in Fig. S3. This bicellular enrichment of PKP1 was significantly reduced upon 14-3-3γ overexpression, whereas 14-3-3σ overexpression did not significantly alter PKP1 distribution between cell contacts and the cytoplasm (Fig. 2E). To illustrate the enrichment of PKP1 at bicellular contacts more directly, individual scans of PKP1 fluorescence intensities of 30 cells were normalized to the mean cytoplasmic value of the respective line scan. Histograms depict the mean distribution of relative PKP1 fluorescence intensities across these line scans (see Fig. S3 for detailed explanation). Comparison of the histograms from control and 14-3-3γ-overexpressing cells clearly demonstrates that cell contact enrichment of PKP1 was considerably reduced in the 14-3-3γ transfected cells (Fig. S4A).

Evaluation of PKP3 fluorescence images suggested a reduced accumulation of PKP3 at tricellular compared to lateral contacts after 14-3-3γ overexpression. To validate this, we measured fluorescence intensities across a line covering the cytoplasm, tricellular and bicellular contacts as indicated in Fig. 2F and Fig. S3A. The histograms derived from 30 line scans confirmed a reduction of the ratio of tricellular to bicellular fluorescence intensities after 14-3-3γ overexpression (Fig. S4B). In agreement, the ratio of tricellular to bicellular fluorescence intensities was significantly lower in 14-3-3γ-overexpressing cells compared to control transfected cells (Fig. 2F; see Fig. S3 for explanation of the procedure). Overexpression of 14-3-3σ did not alter PKP3 distribution between lateral and tricellular contacts (Fig. S4B) as confirmed by calculating the ratio of fluorescence intensities at tricellular versus bicellular contacts (Fig. 2F).

14-3-3γ depletion (see Fig. S5A,B for knockdown efficiency) had minor effects, and correlated with stronger cell border localization of PKP1 and accumulation of PKP3 at tricellular contacts (Fig. 3A–C; Fig. S5C,D). In 14-3-3σ-knockdown cells, the changes in PKP1 and PKP3 distribution were not significant (Fig. 3A–C; Fig. S5C,D). PKP1 nuclear localization was not affected by 14-3-3 isoform expression.

Taken together, these data suggest that 14-3-3γ and 14-3-3σ might target desmosomal proteins to regulate the intercellular cohesion of keratinocytes.

14-3-3 proteins interact with PKPs in a phosphorylation-dependent manner

In order to substantiate the hypothesis that 14-3-3γ and 14-3-3σ regulate intercellular cohesion through PKP1 and PKP3, we identified 14-3-3 interaction partners by immunoprecipitation of GFP–14-3-3γ and GFP–14-3-3σ (Fig. 4A). 14-3-3γ co-precipitated with PKP1. A weak interaction with DSP was also detected, although this could represent an indirect association via PKP1. 14-3-3σ co-precipitated preferentially with PKP3, in agreement with a previous report (Roberts et al., 2013), but in addition revealed a weaker association with PKP1.

14-3-3 proteins typically interact with their targets by binding to specific pS/T motifs that correspond to AGC-kinase family motifs (which includes PKA) (Johnson et al., 2010). Therefore, we asked whether the interaction of 14-3-3 isoforms with PKPs was dependent on phosphorylation. We note that phosphorylation of PKP3-S285 has been previously identified as being essential for complex formation with 14-3-3σ (Roberts et al., 2013), although the physiological context that leads to phosphorylation of this residue was not determined.

We have described that PKP1 is regulated by insulin/IGF1-signaling (Wolf et al., 2013), which often generates 14-3-3 binding sites (Chen et al., 2011). Based on our previous findings that PKP1 is a substrate of Akt2 (Wolf et al., 2013), we overexpressed constitutive active myr–Akt2 in HEK293 cells to induce PKP1 phosphorylation. The activity of Akt2 was confirmed by measuring the increase in phosphorylated eIF4B. Immunoprecipitated FLAG–PKP1 was analyzed for phosphorylation by using an antibody against the motif targeted by AGC kinases (phospho-PKA substrate antibody, RRxpS/T) (Wolf et al., 2013) and for co-precipitation of 14-3-3 proteins (Fig. 4B). In immunoprecipitates from serum-starved HEK293 cells, PKP1 was neither phosphorylated at PKA motifs nor did it co-precipitate with 14-3-3 isoforms, whereas phosphorylation as well as 14-3-3 co-precipitation was observed in Akt2-expressing cells. This suggested a phosphorylation-dependent interaction between PKP1 and 14-3-3 proteins.

To validate these findings, we compared the effects of 14-3-3 expression in keratinocytes kept in serum-free versus those in serum-containing medium. To avoid artifacts caused by PKP1 overexpression, and facilitate PKP1 detection at desmosomes and in the cytoplasm at the same time, we used PKP1-knockout (KO) keratinocytes expressing PKP1–GFP (Keil et al., 2016). Whereas the PKP1–GFP distribution was essentially unaltered by 14-3-3γ or 14-3-3σ in serum-starved cells, 14-3-3γ overexpression induced a redistribution of PKP1–GFP into the cytoplasm in keratinocytes cultured in complete medium (Fig. 4C,D; Fig. S6A–C) confirming our hypothesis that the PKP1–14-3-3 interaction depends on growth factor-mediated signaling. These data support our conclusion that the PKP1–14-3-3γ interaction requires PKP1 phosphorylation.

14-3-3γ and 14-3-3σ differentially regulate adhesion via PKP1 and PKP3

Our data suggest that 14-3-3γ acts preferentially through PKP1. In order to test more directly whether the 14-3-3γ-mediated changes in desmosomal adhesion depend on PKP1, we compared the effects of 14-3-3γ overexpression in wild-type (WT) and PKP1-KO keratinocytes. DSP was used to identify desmosomes in both cells. Compared to WT keratinocytes, PKP1-KO cells revealed, in general, a reduced DSP membrane association along with an increased cytoplasmic pool (see also Rietscher et al., 2016). This distribution was retained after 14-3-3γ overexpression in PKP1-KO cells (Fig. 5A,B). No significant changes were observed in the enrichment of DSP at bicellular contacts (Fig. 5C). In contrast, DSP was redistributed to the cytoplasm in 14-3-3γ-overexpressing WT cells compared to control transfected WT cells, as indicated by a significant reduction of the ratio of bicellular to cytoplasmic fluorescence intensities (Fig. 5A–C; Fig. S7). The lack of 14-3-3γ-induced changes in the DSP distribution in PKP1-KO cells suggests that the role of 14-3-3γ in destabilizing desmosomal adhesion depends at least in part on PKP1.

In contrast, 14-3-3σ overexpression led to an increase in DSP membrane association in PKP1-KO cells, whereas DSP showed a strong plasma membrane association with or without 14-3-3σ overexpression in WT cells (Fig. 5A–C; Fig. S7). This suggests that the stabilizing effects of 14-3-3σ do not critically depend on PKP1, supporting our assumption that 14-3-3σ acts preferentially via PKP3.

In order to further validate the conclusion that 14-3-3γ acts primarily through PKP1, we compared intercellular cohesion of WT

Journal of Cell Science (2018) 131, jcs212191. doi:10.1242/jcs.212191

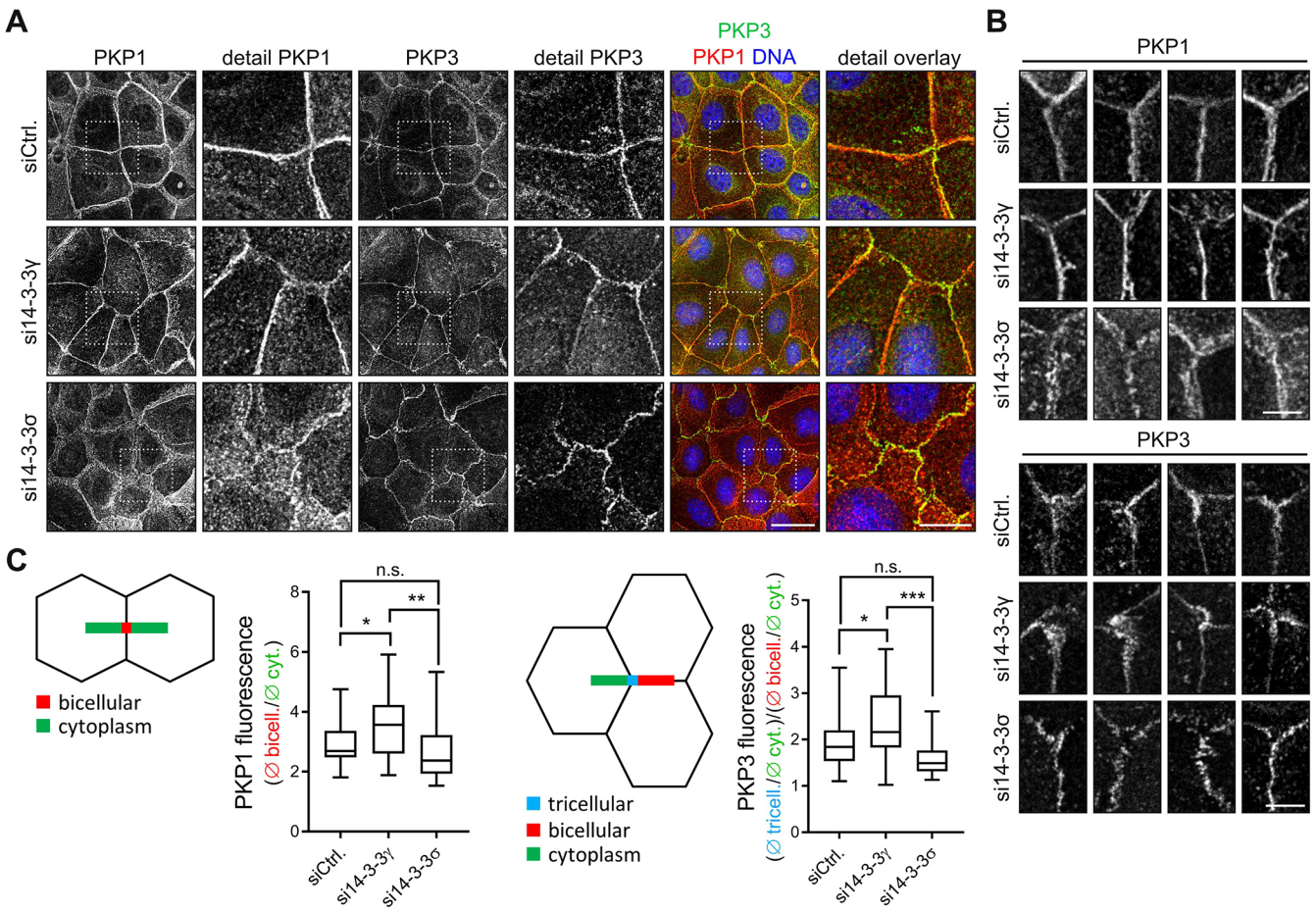

Fig. 3. 14-3-3γ and 14-3-3σ knockdown have opposing effects on the localization of PKP1 and PKP3 in mouse keratinocytes. (A) Mouse keratinocytes transfected with control, 14-3-3γ or 14-3-3σ siRNAs (si14-3-3γ and si14-3-3σ) were switched to HCM at 24 h after transfection, kept in HCM for another 24 h, fixed using MeOH at −20°C and immunostained for PKP1 and PKP3. Confocal images of single optical sections show PKP1 and PKP3 localization in 14-3-3γ and 14-3-3σ knockdown cells. The knockdown of 14-3-3γ was compatible with the segregation of PKP1 and PKP3 to lateral and tricellular contacts, respectively. Knockdown of 14-3-3σ revealed a slightly increased lateral localization of PKP3 and a somewhat more diffuse localization of PKP1. Scale bars: 50 µm (main images), 10 µm (detail images). (B) Details from confocal images of single optical sections emphasize the localization of PKP1 and PKP3 at bicellular and tricellular contacts after knockdown of 14-3-3γ or 14-3-3σ. Scale bars: 6.6 µm. (C) For quantification, PKP1 and PKP3 fluorescence intensities were determined with ImageJ by measuring a segment of equal length and width across 30 individual bicellular or tricellular contacts as illustrated by the colored bars in the schematics. For each line scan the mean junctional (bicellular, red; tricellular, blue) value was normalized to the mean cytoplasmic value (green). The boxplots (whiskers represent the range) reveal a slight enrichment of PKP1 at bicellular contacts in 14-3-3γ knockdown cells, whereas 14-3-3σ knockdown did not lead to significant changes of PKP1 distribution. The ratio of tricellular versus bicellular PKP3 was slightly increased in 14-3-3γ knockdown cells, whereas 14-3-3σ knockdown did not induce significant changes. Knockdown of 14-3-3γ and 14-3-3σ had opposing effects on PKP1 and PKP3 localization. *P<0.05; **P<0.005; ***P<0.0001; n.s., not significant (one-way ANOVA with Tukey's multiple comparisons test).

and PKP1-KO cells by means of a dispase assay. As described previously, intercellular cohesion is considerably reduced in PKP1-KO keratinocytes (Rietscher et al., 2016). Overexpression of 14-3-3γ destabilized the WT keratinocyte sheet (Fig. 5D; see also Fig. 1C), but did not further weaken intercellular cohesion in PKP1-KO cells (Fig. 5D). However, 14-3-3σ slightly stabilized intercellular cohesion in the absence of PKP1 (Fig. 5D), in agreement with the improved membrane association of DSP (Fig. 5A–C), again indicating that this function does not critically depend on PKP1.

To confirm our assumption that 14-3-3σ acts primarily via PKP3, we used PKP3-KO keratinocytes in the dispase assay. Knockdown of 14-3-3σ decreased the mechanical resistance of WT keratinocytes (Fig. 5E, see also Fig. 1C), but not of PKP3-KO keratinocytes. Taken together, these data indicate that the role of 14-3-3γ in destabilizing keratinocyte cohesion depends on PKP1, whereas the impact of 14-3-3σ on desmosomes appears to be primarily mediated by PKP3.

Insulin/Akt2-dependent phosphorylation regulates the PKP1–14-3-3γ association

Since the PKP1–14-3-3 interaction appeared to be phosphorylation dependent (Fig. 4B,C), we asked how insulin/Akt2 signaling promotes this interaction. Prediction tools (http://scansite.mit.edu) identified five pS/T-sites as putative 14-3-3-binding motifs (Fig. 6A). Whereas S54, S118, S119 and T171 are directly phosphorylated by Akt2 *in vitro*, S155 phosphorylation has only been observed in cells expressing active Akt2 (Wolf et al., 2013) suggesting that S155 phosphorylation depends either on a kinase that acts downstream of Akt2 such as, for example, an S6-kinase family member, or that its phosphorylation depends on a specific conformation of PKP1 in a protein complex.

We expressed S/T to A mutants of all predicted PKP1 14-3-3-binding sites in HEK293 cells together with either a control plasmid or myr–Akt2 and incubated cell lysates with GST–14-3-3γ to identify the phosphorylation site that is required for PKP1–14-3-3γ

Journal of Cell Science (2018) 131, jcs212191. doi:10.1242/jcs.212191

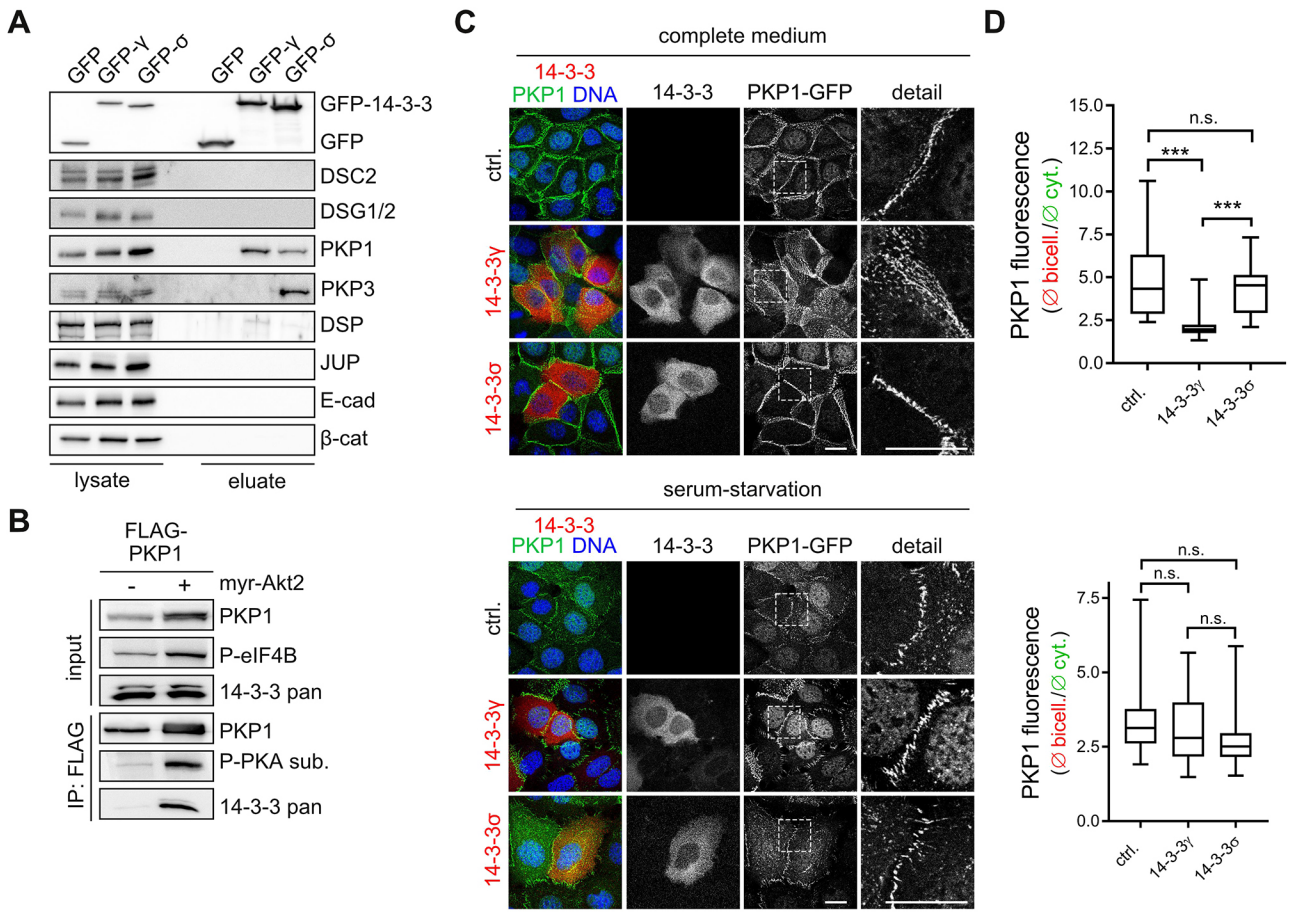

Fig. 4. Growth factor signaling controls the PKP1-14-3-3 association. (A) Mouse keratinocytes transfected with GFP–14-3-3γ (GFP-γ), GFP–14-3-3σ (GFP-σ) or GFP were grown in HCM for 24 h, lysed and incubated with GFP-trap agarose. Lysates and eluates were probed by western blotting with the indicated antibodies. GFP–14-3-3γ interacted with PKP1 but not with PKP3, whereas GFP–14-3-3σ preferentially interacted with PKP3 and to a lesser extent with PKP1. (B) Lysates of serum-starved HEK293 expressing FLAG–PKP1 with or without constitutively active myr–Akt2 as indicated were used for FLAG co-IPs. P-eIF4B confirms phosphorylation of Akt targets. Phosphorylation of precipitated PKP1 at S118 was determined using a phospho-PKA-substrate antibody that recognizes RRxpS/T motifs (Wolf et al., 2013). Co-precipitated 14-3-3 proteins were detected using a pan anti-14-3-3 antibody. 14-3-3 proteins were almost completely absent in immunoprecipitates from serum-starved cells. (C) PKP1-KO keratinocytes expressing PKP1–GFP were transfected with the indicated 14-3-3–Cherry constructs, followed by 12 h of serum stimulation (complete medium, upper part) or serum starvation (lower part) in HCM, and fixed using formaldehyde. Depicted are confocal images of single optical sections showing the localization of PKP1–GFP and 14-3-3-proteins tagged with the red fluorescent protein Cherry. Scale bars: 20 µm. In serum-stimulated cells, PKP1–GFP was redistributed from lateral contacts into the cytoplasm upon 14-3-3γ overexpression, whereas serum depletion abolished this effect. (D) PKP1–GFP distribution was quantified by measuring the fluorescence intensities of segments of equal length and width across 30 individual bicellular contacts for each condition. For each line scan, the mean junctional value was normalized to the mean cytoplasmic value. The boxplots (whiskers represent the range) depict the enrichment factors for GFP–PKP1 at bicellular contacts. *P<0.05; **P<0.005; ***P<0.0001; n.s., not significant (one-way ANOVA with Tukey's multiple comparisons test).

interaction. The S155A mutation almost completely abolished the interaction with 14-3-3γ, and S118A/S119A reduced the association, whereas PKP1 with S54A and T171A mutations still bound to 14-3-3γ and complex formation was increased by Akt2 expression (Fig. 6B). This identifies PKP1-S155 as an essential binding site for 14-3-3γ. S118/S119 might provide a second binding site for the 14-3-3 dimer. Such a bidentate binding mode might dramatically improve complex stability (Sluchanko, 2018) and lead to the preferential binding of 14-3-3γ to PKP1 in the presence of other putative binding partners in the cell.

14-3-3γ sequesters PKP1 in the cytoplasm

14-3-3 proteins can regulate target proteins by controlling their intracellular localization (Obsilova et al., 2014, Aghazadeh and Papadopoulos, 2016). In fact, 14-3-3γ overexpression led to a reduction of cell contact versus cytoplasmic fluorescence intensities, suggesting a shift of PKP1 from desmosomes to the cytoplasm (Fig. 2A,B,E; Fig. S4A). This prompted us to analyze the subcellular localization of the 14-3-3γ–PKP1 complex by using bimolecular fluorescence complementation (BiFC). The BiFC signal confirms that the 14-3-3γ–PKP1 complex localized primarily in the cytoplasm (Fig. 6C). Moreover, this BiFC signal was almost completely lost when 14-3-3γ was co-expressed with PKP1-S155A, confirming that pS155 is essential for the interaction and the cytoplasmic accumulation of PKP1. In contrast, the 14-3-3σ–PKP3 complex localized primarily at the plasma membrane suggesting that complex formation does not interfere with PKP3 incorporation into desmosomes (Fig. 6C). The PKP3-S285A mutant failed to produce a BiFC signal, confirming previous findings that this mutant precludes a 14-3-3σ interaction (Fig. 6C; Roberts et al., 2013).

To further validate the effect on the subcellular localization of PKPs, we quantified the soluble versus insoluble pools (Fig. 7A). 14-3-3γ overexpression significantly increased the cytosolic

Journal of Cell Science (2018) 131, jcs212191. doi:10.1242/jcs.212191

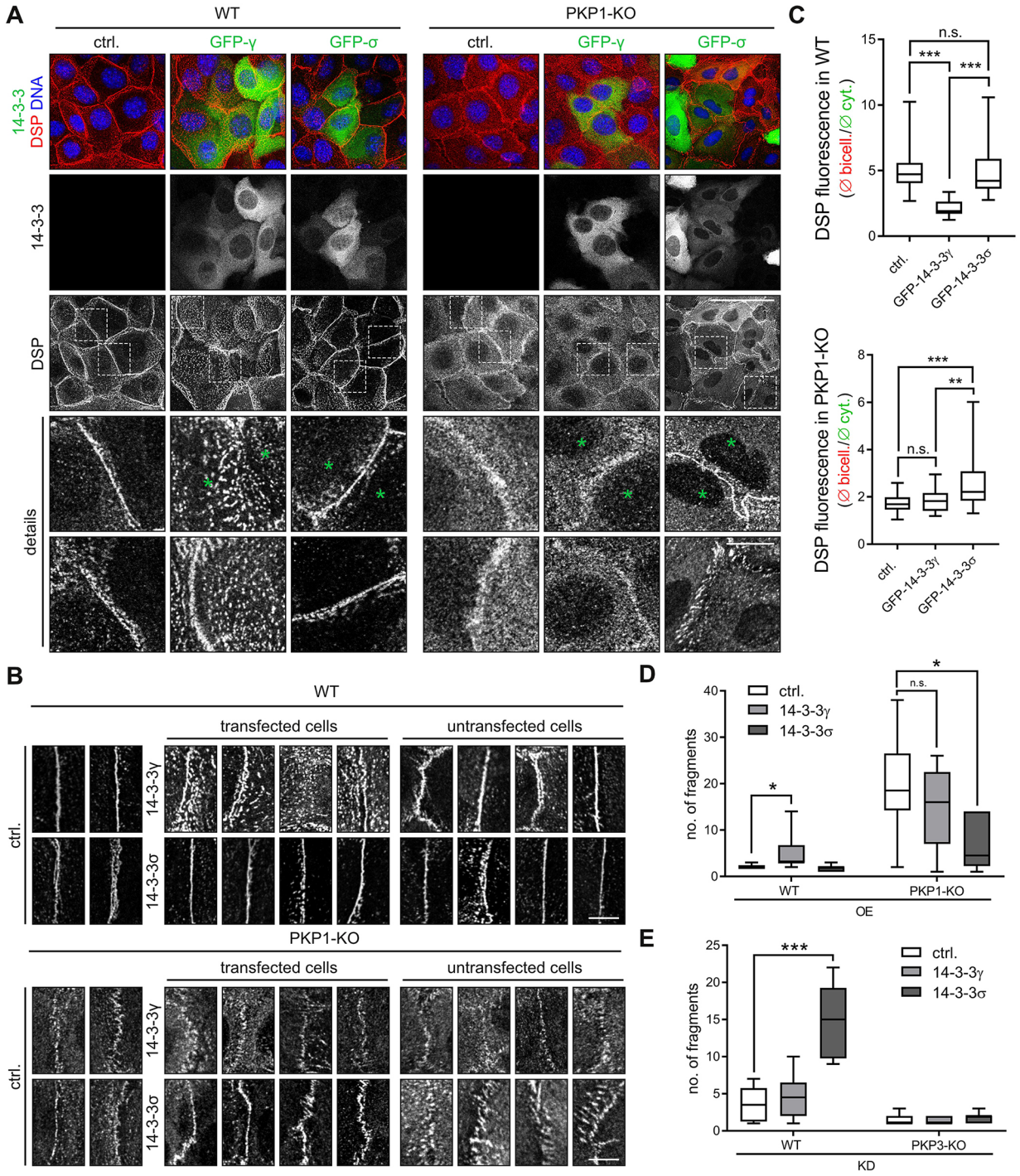

Fig. 5. Intercellular cohesion of keratinocytes is controlled by distinct PKP-14-3-3 complexes. (A) WT and PKP1-KO keratinocytes transfected with the indicated GFP–14-3-3 constructs were grown for 24 h in HCM, fixed using MeOH at −20°C and immunostained for DSP to visualize desmosomes. Depicted are confocal images of single optical sections. Scale bars: 50 µm (main images), 10 µm (detail images). Note that overexpression of 14-3-3σ partially rescued the loss of junctional DSP in PKP1-KO cells. (B) Details from confocal images of single optical sections emphasize the relocalization of DSP at bicellular contacts in transfected versus untransfected cells from the same slide. Scale bars: 6.6 µm. (C) For quantification, DSP fluorescence intensities were determined using ImageJ by measuring a segment of equal length and width across 30 individual bicellular contacts. For each line scan the mean junctional value was normalized to the mean cytoplasmic value. Boxplots (whiskers represent the range) depict the DSP enrichment factors at bicellular contacts. (D,E) WT and PKP1-KO keratinocytes transfected with GFP (control), GFP–14-3-3γ or GFP–14-3-3σ (overexpression, OE, D) or WT and PKP3-KO keratinocytes transfected with control, 14-3-3γ or 14-3-3σ siRNAs (knockdown, KD, E) were kept in HCM for 24 h. The monolayers were then detached using dispase, subjected to mechanical stress through 10 min (PKP1-KO) or 60 min (WT and PKP3-KO) of orbital rotation (300 rpm) and documented using a digital camera. Boxplots depict the number of fragments from eight independent experiments. 14-3-3γ destabilized the epithelial sheet in WT but not in PKP1-KO keratinocytes, whereas 14-3-3σ stabilized cohesion in PKP1-KO cells. The knockdown of 14-3-3σ destabilized intercellular cohesion in WT but not in PKP3-KO cells. **P*<0.05; ***P*<0.005; ****P*<0.0001; n.s., not significant (one-way ANOVA with Tukey's multiple comparisons test).

Journal of Cell Science (2018) 131, jcs212191. doi:10.1242/jcs.212191

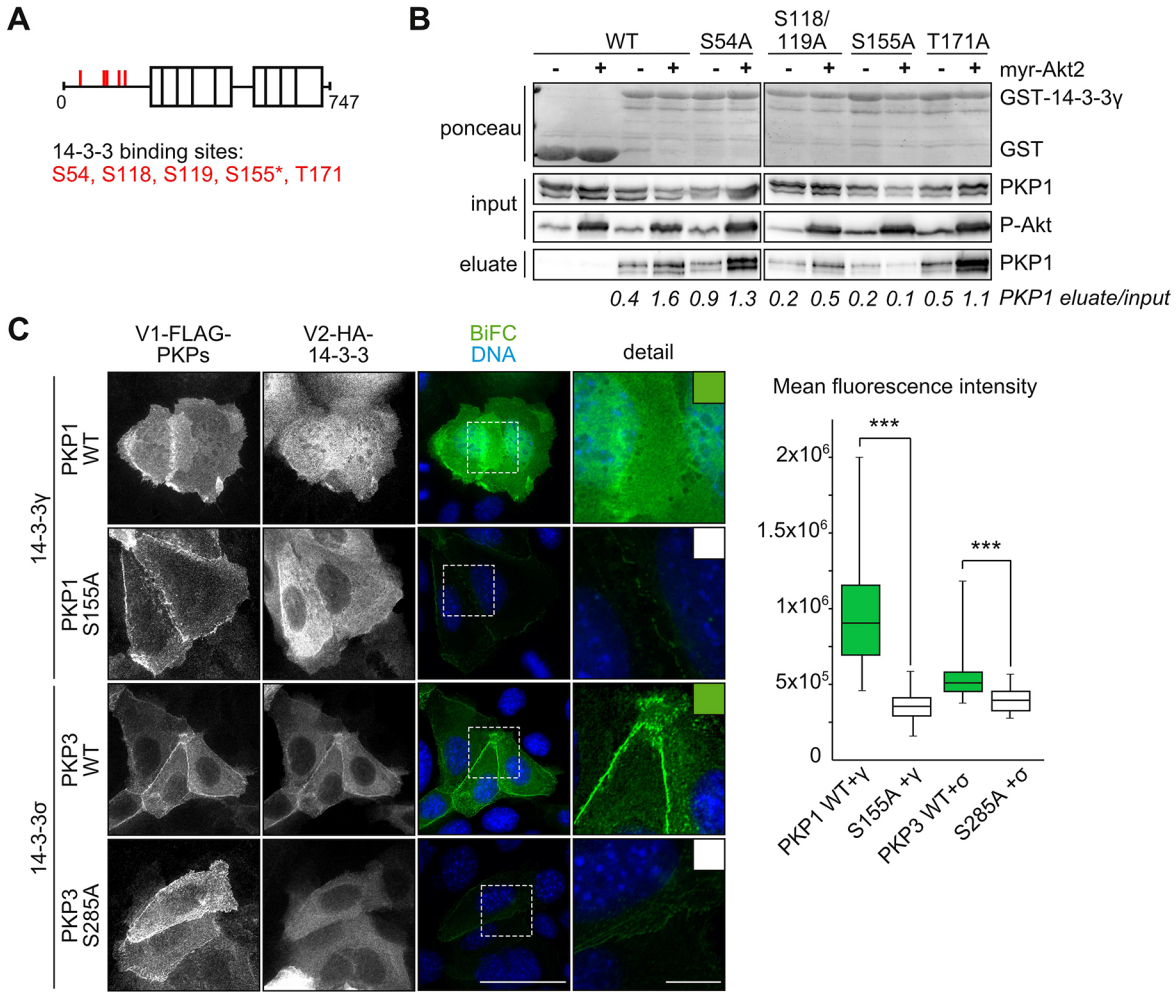

Fig. 6. 14-3-3γ binding to PKP1 depends on S155 phosphorylation. (A) Putative 14-3-3-binding sites in the PKP1 N-terminal domain as predicted by means of the Scansite Motif Scan. S155* indicates an indirect phosphorylation site for Akt2. (B) PKP1-WT and PKP1-S/T mutants were co-expressed with or without constitutive active myr–Akt2 in HEK293 cells as indicated and probed for their interaction with GST–14-3-3γ. Ponceau staining shows equal input of GST–14-3-3γ. GST was used as control. P-Akt confirms the presence of active Akt. PKP1 amounts in the eluate relative to the input are given below the western blot. Mutation of S155 considerably decreased binding of PKP1 to GST–14-3-3γ even in the presence of constitutively active myr–Akt2. (C) Keratinocytes were co-transfected with BiFC constructs as indicated and grown for 24 h in HCM. Co-transfected cells were identified by staining for FLAG (PKPs) and HA epitopes (14-3-3 proteins). Depicted are representative epi-fluorescence microscopy images. The BiFC channel was imaged for an equal exposure time. Scale bars: 50 µm (main images), 10 µm (detail images). The BiFC complex of PKP1-WT and 14-3-3γ is predominantly localized in the cytoplasm, whereas the BiFC complex of PKP3-WT and 13-3-3σ accumulates at intercellular contacts. The PKP1-S155A and the PKP3-S285A mutants abolished the interaction with 14-3-3γ and 14-3-3σ, respectively. For quantification, the mean BiFC intensities of 30 co-transfected cells were determined using ImageJ. ***P<0.0001; n.s., not significant (two-tailed Student's t-test).

fraction of PKP1 but did not affect PKP3 solubility, whereas 14-3-3σ overexpression did not alter the solubility of either PKP. Taken together, these data indicate that the subcellular localization of PKP1 is regulated by 14-3-3γ in a signaling-dependent manner, whereas PKP3 distribution between the cytoplasm and the plasma membrane was unaltered.

14-3-3 proteins modulate PKP dynamics

We hypothesized that 14-3-3γ-mediated cytoplasmic retention of PKP1 correlates with a decreased replacement rate at the desmosome. To test this assumption, we measured the fluorescence recovery after photobleaching (FRAP). In order to avoid artifacts caused by PKP1 overexpression, we used PKP1-KO keratinocytes expressing PKP1–GFP, and characterized PKP1 dynamics by means of FRAP in control-transfected and 14-3-3γ- or 14-3-3σ-depleted cells (Fig. 7B). Knockdown of 14-3-3γ increased PKP1 dynamics at the desmosome, as expected. 14-3-3σ-knockdown had a similar effect, despite its opposing effect on intercellular cohesion. This can be explained by distinct molecular functions: 14-3-3γ sequesters PKP1 in the cytoplasm thereby reducing its exchange rate at the desmosome. This results in a loss of PKP1 from desmosomes and reduced intercellular adhesion. Accordingly, the depletion of 14-3-3γ facilitates PKP1 incorporation into the desmosome and increases its exchange rate. In contrast, 14-3-3σ associates primarily with PKP3 to facilitate its displacement from lateral to tricellular contact sites. Lack of 14-3-3σ increases lateral PKP3 and, as a result, decreases PKP1 stability at the desmosome indirectly. This correlates with slightly increased PKP1 dynamics and decreased intercellular cohesion in 14-3-3σ-knockdown cells.

In a similar approach, we used PKP3-KO keratinocytes expressing PKP3–GFP, and analyzed the effect of 14-3-3γ and 14-3-3σ depletion on PKP3 dynamics. As reported previously, desmosomal PKP3 is more dynamic than PKP1 (Keil et al., 2016). Whereas 14-3-3γ had no significant effect on PKP3–GFP exchange rates at the desmosome, 14-3-3σ depletion led to a minor reduction of PKP3–GFP dynamics (Fig. 7C). This is in apparent contradiction to a

Journal of Cell Science (2018) 131, jcs212191. doi:10.1242/jcs.212191

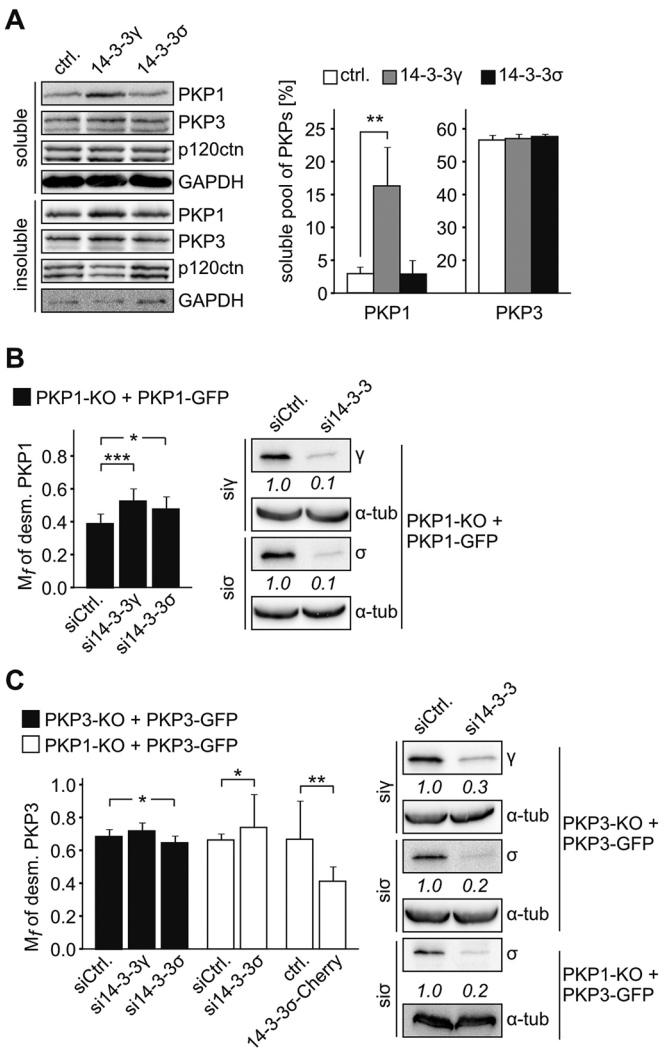

Fig. 7. 14-3-3 proteins differentially modulate PKP dynamics. (A) WT keratinocytes stably expressing GFP–14-3-3γ, GFP–14-3-3σ or GFP (ctrl.) were grown for 24 h in HCM. Triton-X-100-soluble and -insoluble fractions were analyzed by western blotting. GAPDH was used as control for the soluble fraction. The graphs show the relative proportion of PKP1 and PKP3 in the soluble fractions (mean±s.d., n=3). The overexpression of 14-3-3γ significantly increased the solubility of PKP1, whereas PKP3 remained unaffected. In contrast, overexpression of 14-3-3σ neither affected the solubility of PKP1 nor of PKP3. (B,C) PKP1-KO keratinocytes expressing PKP1–GFP (PKP1-KO+PKP1-GFP) or PKP3-GFP (PKP1-KO+PKP3-GFP) and PKP3-KO keratinocytes expressing PKP3-GFP (PKP3-KO+PKP3-GFP) were transfected with the indicated siRNAs (siγ, siσ) or a 14-3-3σ–Cherry expression vector, grown in HCM for 24 h and used for FRAP experiments. The diagrams show the mobile fractions (mean±s.d., n≥10 cells) of desmosomal PKP1–GFP (B) or PKP3–GFP (C) for the indicated conditions. Knockdown efficiencies were determined by western blotting using anti-14-3-3γ and -14-3-3σ antibodies, respectively. α-tubulin is shown as loading control. Knockdown efficiencies normalized to α-tubulin are given below the lanes. *P<0.05, **P<0.005, ***P<0.0001. (Student's t-test for two independent samples two-tailed was used. To compare, ANOVA with Tukey's multiple comparisons test for more than two independent data sets.)

previous report where reduced 14-3-3σ expression lead to an increase in PKP3 dynamics (Roberts et al., 2013). Since the localization of PKP3 at tricellular contacts in mouse keratinocytes depends on PKP1 (Keil et al., 2016), we investigated whether PKP1 expression affects PKP3 dynamics. In order to mimic a PKP1-free situation, we analyzed PKP3–GFP dynamics in PKP1-KO keratinocytes. In fact, 14-3-3σ depletion slightly increased PKP3 dynamics whereas 14-3-3σ overexpression significantly reduced PKP3 exchange rates at lateral desmosomes in the absence of PKP1 (Fig. 7C), in full agreement with a previous report (Roberts et al., 2013).

DISCUSSION

Desmosomes of distinct composition are found in the basal and suprabasal layers of stratified epithelia, and this correlates with the presence of distinct isoforms of desmosomal proteins. Moreover, individual keratinocytes can contain desmosomes of distinct composition, as indicated by the segregation of PKP isoforms with PKP1 preferentially found along lateral contacts and PKP3 accumulating at tricellular contacts (Keil et al., 2016). So far, the mechanisms regulating desmosome dynamics, as well as isoform segregation, are poorly understood. Here, we identify isoform-specific PKP–14-3-3-interactions that modulate PKP dynamics and thereby support the segregation of PKP isoforms to distinct desmosomes. This is essential for keratinocytes to acquire a state of strong intercellular cohesion.

In epithelial cells, specialized tricellular contacts referred to as tricellular tight junctions (tTJs) and tricellular adherens junctions (tAJs) are essential for barrier function, mechano-homeostasis and development. These sites are hot spots of epithelial tension (Higashi and Miller, 2017). Although the molecular components, regulation and function of tTJs and tAJs are beginning to be characterized, the mechanisms responsible for sorting of components to tricellular versus bicellular junctions remain elusive. The tTJ-associated component tricellulin is present along lateral TJs before it segregates into tTJs. We have recently identified PKP3 enriched in tricellular desmosomes, where in analogy to tricellulin, it localized to lateral cell contacts early after cell contact induction, but over time was displaced by PKP1 in differentiating mouse keratinocytes (Keil et al., 2016). Here, we show that sorting of the two PKP isoforms is facilitated by their interactions with 14-3-3 proteins.

We propose that a PKP3–14-3-3σ complex localizes at the lateral plasma membrane, and that this complex facilitates PKP3 exchange in the presence of the less-dynamic PKP1. Since PKP1 is more stable at lateral desmosomes, it out-competes PKP3 along lateral membranes over time. This would result in a slow accumulation of PKP3 at tricellular contact sites along with a gradual depletion from lateral contacts. This would finally promote the high stability of epithelial sheets mediated by lateral PKP1. In agreement with this hypothesis, PKP3 accumulation at tricellular contacts takes at least several hours (Keil et al., 2016). In the absence of PKP1, 14-3-3σ reduces PKP3 exchange at the desmosomes by mediating the retention of the complex at the desmosome, resulting in increased intercellular cohesion that is, however, weaker than cohesion in the presence of PKP1.

Activation of growth factor signaling stimulates proliferation and migration, which requires dynamic remodeling of cell contacts. This is achieved by PKP1 phosphorylation via Akt2, resulting in its accumulation in the cytoplasm and increased activity in promoting translation (Wolf et al., 2013). Phospho-mimetic mutants of PKP1 revealed reduced association with DSP and DSG1 *in vitro*, whereas complex formation with the translation initiation factor eIF4A was not affected (Wolf et al., 2013). In cells, the association of phospho-mimetic PKP1 with the DSG1 cytoplasmic domain was almost completely lost, but binding to eIF4A was again not affected (Wolf et al., 2013). Accordingly, Akt2-dependent phosphorylation of PKP1 interferes with its interaction with DSG1 and thus its incorporation into desmosomes. We propose that 14-3-3γ binding to phosphorylated PKP1 leads to a stabilization of its cytoplasmic pool to prevent its

Journal of Cell Science (2018) 131, jcs212191. doi:10.1242/jcs.212191

desmosomal function and promote its cytoplasmic function. So far it is not known whether phosphorylation takes place at the desmosome to release PKP1 into the cytoplasm where it would be captured by 14-3-3γ to prevent its reincorporation into desmosomes. Alternatively, Akt2 could phosphorylate PKP1 before it is incorporated into desmosomes. The presence of Akt2–PKP1 complexes at the membrane as revealed by BiFC (Wolf et al., 2013) supports the view that Akt2 can target desmosomal PKP1. Owing to the loss of PKP1 from lateral desmosomes, PKP3 would be no longer displaced from the lateral membranes and would become more uniformly distributed, leading to weaker and more dynamic adhesion (Fig. 8).

14-3-3σ expression increases in differentiating keratinocytes, and its overexpression stimulates differentiation (Cianfarani et al., 2011). This correlates with increased intercellular cohesion in suprabasal keratinocytes. Interestingly, our data suggest that 14-3-3σ promotes strong adhesion mediated by PKP1 through an indirect mechanism that targets PKP3. Basal PKP3-S285 phosphorylation facilitates the PKP3–14-3-3σ interaction in a growth factor-independent fashion. By stimulating PKP3 dynamics at the lateral membrane, 14-3-3σ facilitates the accumulation of PKP3 at tricellular contacts and the distribution of PKP1 along lateral membranes, as observed during differentiation and junction maturation (Keil et al., 2016), leading to the model depicted in Fig. 8.

At the mechanistic level, it is not clear how exactly elevated PKP1 expression leads to more stable desmosomes. One mechanism might be that PKP1 either induces the expression or stabilizes DSG1 and DSC1, which are responsible for strong cohesion. Harrison et al. (2016) have systematically analyzed the structural basis of adhesive binding by DSGs and DSCs. Through analytical ultracentrifugation and surface plasmon resonance, these authors determined K_d values for DSG and DSC homodimers as well as heterodimers. The strongest-binding pairs were DSG1–DSC1 and DSG4–DSC1. Thus, PKP1 might regulate adhesive strength by modulating DSG1 and DSC1 levels.

Our results are in good agreement with the reported tumor-suppressive potential of 14-3-3σ and an oncogenic role of 14-3-3γ (Hermeking and Benzinger, 2006; Lodygin and Hermeking, 2006; Morrison, 2009; Radhakrishnan and Martinez, 2010), and suggest that their function in carcinogenesis might in part depend on the control of desmosomal adhesion. Since diminished intercellular adhesion is a hallmark of cancer, we speculate that 14-3-3γ-mediated attenuation of desmosome function contributes to its oncogenic potential in stratified epithelia.

14-3-3 proteins interact with a vast number of proteins, thereby affecting many cellular processes. Among the 14-3-3-regulated proteins are keratins, which are directly anchored at the desmosomes. Therefore, one might expect that their regulation by 14-3-3 proteins is interrelated and that modulation of desmosomes might depend in part on 14-3-3–keratin interactions. However, 14-3-3 proteins associate preferentially with the hyper-phosphorylated cytosolic fraction of keratins during mitosis, to act as solubility cofactors (Liao et al., 1997; Sawant and Leube, 2017), but not with the un-phosphorylated filaments that associate with desmosomes, making a direct link between 14-3-3–keratin complexes and desmosomes unlikely. However, keratin 17 (K17), whose expression is upregulated in stratified epithelia upon wounding, might indirectly affect the 14-3-3-mediated regulation of desmosomes. Phospho-K17 associates with 14-3-3σ to promote the cytosolic retention of 14-3-3σ, which stimulates Akt protein family activity to support cell growth (Kim et al., 2006). This could promote Akt-dependent PKP1 phosphorylation and PKP1–14-3-3γ complex formation, thus attenuating intercellular cohesion to facilitate tissue repair.

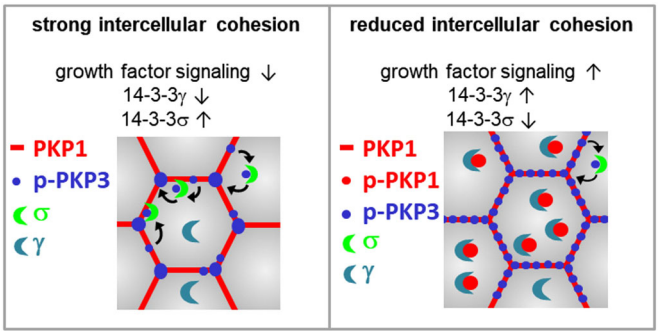

Fig. 8. Hypothetical model depicting the regulation of PKP1 and PKP3 by 14-3-3γ and 14-3-3σ, respectively. Decreased growth factor signaling along with low 14-3-3γ and high 14-3-3σ levels results in strong intercellular cohesion. Basal phosphorylation of PKP3 on S285 permits its interaction with 14-3-3σ in a growth factor-independent fashion and facilitates its displacement from lateral to tricellular contact sites in the presence of PKP1. Since PKP1 is more stable at lateral desmosomes, it out-competes PKP3 along lateral membranes over time which results in an accumulation of PKP3 at tricellular contact sites and strong intercellular cohesion (left). Growth factor-induced phosphorylation of PKP1 enables its interaction with 14-3-3γ, resulting in the retention of the complex in the cytoplasm. Owing to the loss of PKP1 from lateral desmosomes, PKP3 is no longer displaced from the lateral membranes and becomes more uniformly distributed along the membrane leading to weaker and more dynamic cohesion (right).

Taken together, we have identified a hitherto unappreciated and isoform-dependent role of 14-3-3γ and 14-3-3σ in the regulation of desmosome stability that depends on their interaction with PKP isoforms. At a mechanistic level, 14-3-3γ and 14-3-3σ control PKP1 and PKP3 segregation into bicellular and tricellular contacts by regulating PKP dynamics.

MATERIALS AND METHODS

cDNA constructs

Human cDNAs of 14-3-3γ and 14-3-3σ were subcloned into pEGFP-C2 (Takara Bio Inc.), pGEX-5x1 (Amersham Bioscience), pVen2-HA-C2 (Wolf et al., 2006), pmCherry-C1 and pLVX-IRES-puro (Takara Bio Inc.) containing an EGFP open-reading frame (ORF). Human cDNAs of PKP1 and PKP3 were subcloned into pLVX-IRES-puro (Takara Bio Inc.) containing an EGFP ORF. Vectors for production of lentiviral particles pMD2.G and psPAX2 were from Addgene (plasmids #12259, #12260; deposited by Didier Trono). myr-HA-Akt2-pcDNA3 was from Addgene plasmid #9016 (deposited by William Sellers); and pcDNA3 plasmid was purchased from Invitrogen. FLAG–PKP1 constructs were as described previously (Wolf et al., 2010). PKP1 mutants were described in Wolf et al. (2013). PKP1-S155A and PKP3-S285A mutants were generated by *in vitro* mutagenesis. PKP1-WT and PKP3-WT, as well as PKP1 and PKP3 mutants were inserted into pVen1-FLAG-C2 (Wolf et al., 2006).

Antibodies

Primary antibodies used for immunofluorescence analysis and western blotting are listed in Table S1, with the appropriate dilution noted. Secondary antibodies were donkey anti-mouse-, anti-goat- and anti-rabbit-IgG conjugated to horseradish peroxidase and donkey anti-mouse-, anti-guinea pig-, anti-goat- and anti-rabbit-IgG conjugated to Dylight488 or Cy3 (Jackson ImmunoResearch, West Grove, PA, USA).

Cell culture, transfection, RNA interference and treatments

HEK293 cells were grown in Dulbecco's modified Eagle's medium [DMEM, 4.5 g/l high glucose, 1 mM sodium pyruvate, 1 mM glutamate, 10% (v/v) FCS] at 37°C, 5% CO_2 and 90% humidity. Keratinocytes from WT, PKP1-KO (Rietscher et al., 2016) and PKP3-KO mice (a gift from Frans Van Roy; Sklyarova et al., 2008) were isolated from the epidermis of newborn pups

using 0.025% trypsin/0.02% EDTA/PBS essentially as described previously (Kashiwagi and Huh, 2005; Kröger et al., 2013). All animal experiments were performed according to approved guidelines (Landesverwaltungsamt Sachsen-Anhalt, reference number 42502-2-1166 MLU). PKP1- and PKP3-KO keratinocytes expressing PKP1- or PKP3-GFP, respectively, have been described (Keil et al., 2016). To generate WT keratinocytes expressing GFP, GFP–14-3-3γ or GFP–14-3-3σ, HEK293T cells were co-transfected by $CaPO_4$ precipitation with pMD2.G, psPAX2 and pLVX-IRES-puro, containing human 14-3-3γ or 14-3-3σ. Lentiviral particles were purified 48 h after transfection by using a Lenti-X concentrator (Takara Bio Inc.) according to the manufacturer's protocol. Mouse keratinocytes were incubated with the lentiviral particles for 24 h and selected with puromycin. The cells were grown on collagen I in low calcium medium [LCM; DMEM/Ham's F12 medium containing 50 µM $CaCl_2$, 10% (v/v) Ca^{2+}-free FCS, 1 mM sodium pyruvate, 1 mM glutamate, 0.18 mM adenine, 0.5 µg/ml hydrocortison, 5 µg/ml insulin, 10 ng/ml EGF, 100 pM cholera toxin] at 32°C, 5% CO_2 and 90% humidity. To induce differentiation of keratinocytes, cells were switched to 1.2 mM Ca^{2+}-containing LCM (HCM) for 24 h to 6 days. For growth factor stimulation, keratinocytes were maintained in serum-free (without FCS, insulin, EGF and cholera toxin) LCM for 24 h and stimulated with complete medium (HCM) for 12 h. Transfection of plasmid DNA was performed using Xfect™ (Clontech) according to the manufacturer's protocol. For knockdown analysis in mouse keratinocytes, siRNAs were transfected with Lipofectamine® RNAiMax (Thermo Fisher Scientific) according to the manufacturer's protocol. siRNA pools (defined pools of 30 selected siRNAs) used in this study were generated by siTools Biotech GmbH (Martinsried, Germany). At 24 h after transfection of DNA or siRNAs, respectively, cells were switched to HCM.

Protein lysate preparation from mouse skin and cells, SDS-PAGE and western blotting

For analysis of protein expression, pieces of dorsal skin from newborn mice were homogenized with a T25 ULTRA-TURRAX (IKA, Staufen, Germany) and boiled for 5 min in SDS-sample buffer (20 mM Tris-HCl pH 7.5, 1% SDS, supplemented with 1 µg/ml aprotinin, 1 µg/ml leupeptin, 1 mM Pefabloc, 5 mM NaF and 1 mM $NaVO_3$). Skin extracts were centrifuged for 15 min at 13,000 ***g***. Mouse keratinocytes were suspended in SDS sample buffer, boiled for 5 min and centrifuged for 15 min at 13,000 ***g***. Total protein concentration was determined by using the BCA Protein Assay Kit (Thermo Scientific). Equal amounts of protein were separated by SDS-PAGE and transferred to nitrocellulose. The transferred proteins were monitored by staining the membrane with 1× Ponceau S [2% (w/v) Ponceau S, 30% (w/v) trichloroacetic acid (TCA) and 30% (w/v) sulfosalicylic acid] for 10 min. The membrane was briefly washed in 1× TBST (Tris-buffered saline with 0.1% Tween20), incubated with blocking solution [5% (w/v) skimmed milk in TBST] and probed with the appropriate antibodies. Chemiluminescence was detected via the Fusion-SL 3500.WL imaging system (Peqlab; Erlangen, Germany). α-tubulin or vinculin were used as loading controls.

Solubility assay

Mouse keratinocytes stably expressing GFP, GFP–14-3-3γ or GFP–14-3-3σ, respectively, were suspended for 15 min in non-denaturing lysis buffer (20 mM Tris-HCl pH 7.6, 140 mM NaCl, 10% glycerol, 1.5% Triton X-100, 2 mM EDTA, 10 µg/ml aprotinin, 10 µg/ml leupeptin, 1 mM PefaBloc, 1 mM NaF, 1 mM $NaVO_3$). After centrifugation for 30 min at 13,000 ***g***, the supernatant (soluble fraction) was collected and the pellet (insoluble fraction) was resuspended in the same volume of 20 mM Tris-HCl pH 7.5, and 1% SDS supplemented with 1 µg/ml aprotinin, 1 µg/ml leupeptin, 1 mM Pefabloc, 5 mM NaF and 1 mM $NaVO_3$, and fractions were resolved by SDS-PAGE, transferred to nitrocellulose and probed with the appropriate antibodies.

GST pulldown

14-3-3γ in pGEX-5x1 (Amersham) and pGEX-5x1 (control) were expressed in *Escherichia coli* BL21DE3. Bacteria were harvested by centrifugation at 1000 ***g***, resuspended in lysis buffer (20 mM HEPES pH 7.5, 150 mM NaCl, 1 mM EDTA, 10 µg/ml aprotinin, 10 µg/ml leupeptin, 1 mM PefaBloc and 1 mM dithiothreitol) and sonicated. Triton X-100 was added to a final concentration of 1% (v/v) and the lysates were incubated for 30 min at 4°C. The cleared lysates were incubated with Glutathione–agarose (Pierce Biotechnology) for 1 h at 4°C. The concentration of bound glutathione S-transferase (GST)–14-3-3γ and GST (control) was determined using Coomassie Plus protein reagent (Pierce). For GST pulldown, 500 µl of HEK293 lysates were added to 30 µl GST– or GST–14-3-3γ–agarose, respectively, and incubated for 2 h at 4°C. Bound protein was eluted in SDS-PAGE loading buffer, separated on SDS gels and analyzed by western blotting.

FLAG and GFP immunoprecipitation

For FLAG immunoprecipitation, HEK293 cells expressing FLAG–PKP1 in the presence or absence of myr–HA–Akt2 were lysed in buffer containing 50 mM Tris-HCl pH 7.4, 150 mM NaCl, 1% NP-40, 0.25% sodium deoxycholate, 1 mM EDTA, 1 mM EGTA, 10 µg/ml aprotinin, 10 µg/ml leupeptin, 1 mM PefaBloc, 1 mM NaF and 1 mM $NaVO_3$. Lysates were cleared by centrifugation for 15 min at 4°C and 13,000 ***g*** and subsequently incubated with anti-FLAG M2 affinity gel (Sigma). Bound proteins were solubilized in SDS-PAGE loading buffer, separated by SDS-PAGE and analyzed by western blotting.

For the GFP-trap®, mouse keratinocytes expressing GFP, GFP–14-3-3γ or GFP–14-3-3σ, respectively, were lysed in buffer containing 10 mM Tris-HCl pH 7.5, 150 mM NaCl, 0.5 mM EDTA, 0.5% (v/v) NP-40, 10 µg/ml aprotinin, 10 µg/ml leupeptin, 1 mM pefabloc, 1 mM DTT, 5 mM NaF and 1 mM $NaVO_3$. Lysates were cleared by centrifugation for 15 min at 4°C and 13,000 ***g***, and subsequently incubated with GFP-trap® beads (ChromoTek). Bound proteins were solubilized in SDS-PAGE loading buffer, separated by SDS-PAGE and analyzed by western blotting.

Dispase assay

For analysis of intercellular cohesion, mouse keratinocytes were seeded onto 12-well plates, grown to confluence and switched to 1.2 mM Ca^{2+} for 24 h. Cells were washed twice in PBS (+1.2 mM Ca^{2+}) and incubated for 30 min with dispase II (Roche Diagnostics, 5 U/ml) in keratinocyte medium containing 1.2 mM Ca^{2+} at 37°C/5% CO_2. Free floating monolayers were shaken on an orbital shaker for 10 min for PKP1-KO, or 1 h for WT and PKP3-KO keratinocytes at room temperature, and images were taken using a Sony DSC-H300 camera. ImageJ was used for image processing and counting of fragments.

Immunofluorescence analysis

Mouse keratinocytes grown on collagen I-coated coverslips were fixed for 10 min in methanol at −20°C or for 15 min in 3.7% (w/v) formaldehyde in PBS, permeabilized in 0.5% (v/v) Triton X-100 in PBS for 15 min at room temperature and blocked in 1% BSA in PBS for 30 min at room temperature. Antibodies were diluted in 1% (w/v) BSA in PBS and incubated overnight at 4°C in a humid chamber. DNA was stained with Hoechst 33342 (Thermo Fisher Scientific). Coverslips were mounted in Mowiol. BiFC images and images of endogenous 14-3-3γ and 14-3-3σ were taken using a Zeiss Axio Observer.Z1 microscope equipped with the Zeiss ApoTome, a CDD camera (AxioCam MRm Rev. 3) and either a Plan-Apochromat 63×1.40 NA oil DIC or a Plan-Apochromat 20×0.8 NA objective, controlled with the AxioVision Rel. 4.7 software. Confocal images were taken with a Leica-TSC SP5 AOBS confocal microscope using a HCX PL APO Lambda Blue 63.0×/1.40 oil and HCX PL APO Lambda Blue 40×/1.25-0.75 oil objective.

ImageJ was used for image processing. To determine the enrichment factors for PKP1 or DSP at bicellular contacts, PKP1 or DSP fluorescence intensities were measured in segments of equal length and width covering the cytoplasm and bicellular contacts as illustrated in Fig. S3A. The enrichment factors for PKP1 and DSP at bicellular contacts were calculated by dividing the mean junctional value of each line scan by the corresponding mean cytoplasmic value for a total of 30 individual measurements.

To quantify the accumulation of PKP3 at tricellular contacts, PKP3 fluorescence intensities were measured in segments of equal length and width covering the cytoplasm, bicellular and tricellular contacts as illustrated in Fig. S3A. The mean bicellular and tricellular PKP3 fluorescence intensities were normalized to the corresponding mean cytoplasmic values for each line scan. The normalized tricellular value was divided by the normalized bicellular value for a total of 30 individual measurements to calculate the

mean enrichment factor for PKP3 at tricellular compared to bicellular contacts.

All calculated enrichment factors are shown as boxplots displaying the first to third quartile with the full range of variation (Fig. S3B). To depict the mean distribution of PKP1, DSP and PKP3 along the line scans, fluorescence intensities along the line scans were normalized to the corresponding mean cytoplasmic value. To compare control versus treated cells, line scans of 30 individual intercellular contacts were averaged, resulting in histograms depicting the mean relative fluorescence intensities (Fig. S3C). Statistical significances between the mean bicellular and tricellular values were determined using a one-way ANOVA followed by a Tukey's multiple comparison test.

BiFC

For BiFC analysis, mouse keratinocytes were co-transfected with the indicated pVen1 and pVen2 constructs. At 4 h after transfection, LCM was switched to HCM, and cells were incubated for 12 h before fixation in 3.7% (w/v) formaldehyde in PBS and immunostaining with FLAG- and HA-tag-directed antibodies. DNA was stained with Hoechst 33342 (Thermo Fisher Scientific). Coverslips were mounted in Mowiol. Images of cells expressing both FLAG- and HA-tagged fusion proteins were taken with identical exposure times (1500 ms) to enable a comparison of BiFC efficiencies. Image processing and the mean BiFC fluorescence intensities of two adjacent cells (n=30 images) were undertaken using ImageJ.

FRAP measurements

The dynamics of PKP1– and PKP3–GFP in PKP1- and PKP3-KO keratinocytes transfected with siRNAs or 14-3-3σ–Cherry were analyzed by FRAP 24 h after addition of 1.2 mM Ca^{2+}. Bleaching and imaging was performed on a confocal microscope (TCS SP5; Leica) using an oil-immersion 63× objective (HCX PL APO Lambda Blue, NA 1.4) and an argon laser at 488 nm. Five images were taken before the bleach pulse and 200 images after bleaching with an image acquisition frequency of ∼2 frames/s. For data analysis, the fluorescence intensities from three regions of interest per cell (ROI1=bleached intercellular contact, ROI2=total cell and ROI3=background) were determined. For each time point, the background intensity was subtracted and the data were full scale normalized using the following formula based on the easyFRAP tool (Rapsomaniki et al., 2012):

$$I(t)^{dn} = \left[\left(\frac{1}{n\,pre}\times\sum_{t=1}^{n\,pre} I(t)ROI2'\right) \div I(t)ROI2'\right] \times \left[I(t)ROI1' \div \left(\frac{1}{n\,pre}\times\sum_{t=1}^{n\,pre} I(t)ROI1'\right)\right],$$

$$I(t)^{fullscale} = [(I(t)^{dn} - I(t_{postbleach})^{dn}] \div [1 - I(t_{postbleach})^{dn}]$$

where I=fluorescence intensity; t=time; dn=double normalized; and $ROI1'$/$ROI2'$=background-subtracted ROIs.

The fluorescence recovery curve was fitted to a single exponential function: $I(t)=A(1-e^{-\tau t})$, where $I(t)$ is the intensity at time t, A the plateau level after recovery (mobile fraction) and τ the slope of the exponential term (time constant).

Statistical analysis

All statistical analyses were performed using GraphPad Prism7. Error bars represent standard deviations (s.d.). For two independent samples, statistically significant differences were determined with a two-tailed Student's t-test. To compare more than two independent data sets with normal distribution, one-way analysis of variance (ANOVA) followed by a Tukey's multiple comparison test was used. Asterisks indicate statistical significance (*P<0.05, **P<0.005, ***P<0.0001).

Acknowledgements

We thank Annika Wolf for her contribution in an initial phase of the project and Andrej Mun for technical assistance. We are grateful to the core facility imaging for support.

Competing interests

The authors declare no competing or financial interests.

Author contributions

Conceptualization: M.H., K.R., R.K.; Methodology: K.R., R.K., M.H.; Validation: K.R., R.K.; Formal analysis: K.R., R.K.; Investigation: K.R., R.K., A.J.; Resources: M.H.; Data curation: K.R., R.K.; Writing - original draft: M.H.; Writing - review & editing: K.R., R.K., M.H.; Visualization: K.R., R.K.,; Supervision: M.H.; Project administration: M.H.; Funding acquisition: M.H.

Funding

The project was supported by Deutsche Forschungsgemeinschaft grants to M.H. (Ha1791/8-1 and Ha1791/10-1, SPP 1782).

Supplementary information

Supplementary information available online at
http://jcs.biologists.org/lookup/doi/10.1242/jcs.212191.supplemental

References

Aghazadeh, Y. and Papadopoulos, V. (2016). The role of the 14-3-3 protein family in health, disease, and drug development. *Drug Discov. Today* **21**, 278-287.

Bass-Zubek, A. E., Godsel, L. M., Delmar, M. and Green, K. J. (2009). Plakophilins: multifunctional scaffolds for adhesion and signaling. *Curr. Opin. Cell Biol.* **21**, 708-716.

Chen, S., Synowsky, S., Tinti, M. and MacKintosh, C. (2011). The capture of phosphoproteins by 14-3-3 proteins mediates actions of insulin. *Trends Endocrinol. Metab.* **22**, 429-436.

Cianfarani, F., Bernardini, S., De Luca, N., Dellambra, E., Tatangelo, L., Tiveron, C., Niessen, C. M., Zambruno, G., Castiglia, D. and Odorisio, T. (2011). Impaired keratinocyte proliferative and clonogenic potential in transgenic mice overexpressing 14-3-3sigma in the epidermis. *J. Invest. Dermatol.* **131**, 1821-1829.

Dellambra, E., Golisano, O., Bondanza, S., Siviero, E., Lacal, P., Molinari, M., D'Atri, S. and De Luca, M. (2000). Downregulation of 14-3-3sigma prevents clonal evolution and leads to immortalization of primary human keratinocytes. *J. Cell Biol.* **149**, 1117-1130.

Fischer-Keso, R., Breuninger, S., Hofmann, S., Henn, M., Rohrig, T., Strobel, P., Stoecklin, G. and Hofmann, I. (2014). Plakophilins 1 and 3 bind to FXR1 and thereby influence the mRNA stability of desmosomal proteins. *Mol. Cell. Biol.* **34**, 4244-4256.

Harrison, O. J., Brasch, J., Lasso, G., Katsamba, P. S., Ahlsen, G., Honig, B. and Shapiro, L. (2016). Structural basis of adhesive binding by desmocollins and desmogleins. *Proc. Natl. Acad. Sci. USA* **113**, 7160-7165.

Hatzfeld, M. (2007). Plakophilins: multifunctional proteins or just regulators of desmosomal adhesion? *Biochim. Biophys. Acta Mol. Cell Res.* **1773**, 69-77.

Hatzfeld, M., Wolf, A. and Keil, R. (2014). Plakophilins in desmosomal adhesion and signaling. *Cell Commun. Adhes.* **21**, 25-42.

Hatzfeld, M., Keil, R. and Magin, T. M. (2017). Desmosomes and intermediate filaments: their consequences for tissue mechanics. *Cold Spring Harb. Perspect. Biol.* **9**, a029157.

Hermeking, H. and Benzinger, A. (2006). 14-3-3 proteins in cell cycle regulation. *Semin. Cancer Biol.* **16**, 183-192.

Herron, B. J., Liddell, R. A., Parker, A., Grant, S., Kinne, J., Fisher, J. K. and Siracusa, L. D. (2005). A mutation in stratifin is responsible for the repeated epilation (Er) phenotype in mice. *Nat. Genet.* **37**, 1210-1212.

Higashi, T. and Miller, A. L. (2017). Tricellular junctions: how to build junctions at the TRICkiest points of epithelial cells. *Mol. Biol. Cell* **28**, 2023-2034.

Johnson, C., Crowther, S., Stafford, M. J., Campbell, D. G., Toth, R. and MacKintosh, C. (2010). Bioinformatic and experimental survey of 14-3-3-binding sites. *Biochem. J.* **427**, 69-78.

Kashiwagi, M. and Huh, N. H. (2005). Organ culture of developing mouse skin and its application for molecular mechanistic studies of morphogenesis. *Methods Mol. Biol.* **289**, 39-46.

Keil, R., Rietscher, K. and Hatzfeld, M. (2016). Antagonistic regulation of intercellular cohesion by Plakophilins 1 and 3. *J. Invest. Dermatol.* **136**, 2022-2029.

Kim, S., Wong, P. and Coulombe, P. A. (2006). A keratin cytoskeletal protein regulates protein synthesis and epithelial cell growth. *Nature* **441**, 362-365.

Kowalczyk, A. P. and Green, K. J. (2013). Structure, function, and regulation of desmosomes. *Prog. Mol. Biol. Transl. Sci.* **116**, 95-118.

Kröger, C., Loschke, F., Schwarz, N., Windoffer, R., Leube, R. E. and Magin, T. M. (2013). Keratins control intercellular adhesion involving PKC-alpha-mediated desmoplakin phosphorylation. *J. Cell Biol.* **201**, 681-692.

Li, Q., Lu, Q., Estepa, G. and Verma, I. M. (2005). Identification of 14-3-3sigma mutation causing cutaneous abnormality in repeated-epilation mutant mouse. *Proc. Natl. Acad. Sci. USA* **102**, 15977-15982.

Liao, J., Ku, N.-O. and Omary, M. B. (1997). Stress, apoptosis, and mitosis induce phosphorylation of human keratin 8 at Ser-73 in tissues and cultured cells. *J. Biol. Chem.* **272**, 17565-17573.

Liu, M. Y., Cai, S. L., Espejo, A., Bedford, M. T. and Walker, C. L. (2002). 14-3-3 interacts with the tumor suppressor tuberin at Akt phosphorylation site(s). *Cancer Res.* **62**, 6475-6480.

Lodygin, D. and Hermeking, H. (2006). Epigenetic silencing of 14-3-3sigma in cancer. *Semin. Cancer Biol.* **16**, 214-224.

Morrison, D. K. (2009). The 14-3-3 proteins: integrators of diverse signaling cues that impact cell fate and cancer development. *Trends Cell Biol.* **19**, 16-23.

Obsilova, V., Kopecka, M., Kosek, D., Kacirova, M., Kylarova, S., Rezabkova, L. and Obsil, T. (2014). Mechanisms of the 14-3-3 protein function: regulation of protein function through conformational modulation. *Physiol. Res.* **63**, S155-S164.

Radhakrishnan, V. M. and Martinez, J. D. (2010). 14-3-3gamma induces oncogenic transformation by stimulating MAP kinase and PI3K signaling. *PLoS ONE* **5**, e11433.

Rapsomaniki, M. A., Kotsantis, P., Symeonidou, I.-E., Giakoumakis, N.-N., Taraviras, S. and Lygerou, Z. (2012). easyFRAP: an interactive, easy-to-use tool for qualitative and quantitative analysis of FRAP data. *Bioinformatics* **28**, 1800-1801.

Rietscher, K., Wolf, A., Hause, G., Rother, A., Keil, R., Magin, T. M., Glass, M., Niessen, C. M. and Hatzfeld, M. (2016). Growth retardation, loss of desmosomal adhesion, and impaired tight junction function identify a unique role of Plakophilin 1 in vivo. *J. Invest. Dermatol.* **136**, 1471-1478.

Roberts, B. J., Reddy, R. and Wahl, J. K.III. (2013). Stratifin (14-3-3 sigma) limits plakophilin-3 exchange with the desmosomal plaque. *PLoS ONE* **8**, e77012.

Sambandam, S. A. T., Kasetti, R. B., Xue, L., Dean, D. C., Lu, Q. and Li, Q. (2015). 14-3-3sigma regulates keratinocyte proliferation and differentiation by modulating Yap1 cellular localization. *J. Invest. Dermatol.* **135**, 1621-1628.

Sawant, M. S. and Leube, R. E. (2017). Consequences of keratin phosphorylation for cytoskeletal organization and epithelial functions. *Int. Rev. Cell Mol. Biol.* **330**, 171-225.

Sehgal, L., Mukhopadhyay, A., Rajan, A., Khapare, N., Sawant, M., Vishal, S. S., Bhatt, K., Ambatipudi, S., Antao, N., Alam, H. et al. (2014). 14-3-3gamma-Mediated transport of plakoglobin to the cell border is required for the initiation of desmosome assembly in vitro and in vivo. *J. Cell Sci.* **127**, 2174-2188.

Sklyarova, T., Bonné, S., D'Hooge, P., Denecker, G., Goossens, S., De Rycke, R., Borgonie, G., Bösl, M., van Roy, F. and van Hengel, J. (2008). Plakophilin-3-deficient mice develop hair coat abnormalities and are prone to cutaneous inflammation. *J. Invest. Dermatol.* **128**, 1375-1385.

Sluchanko, N. N. (2018). Association of multiple phosphorylated proteins with the 14-3-3 regulatory hubs: problems and perspectives. *J. Mol. Biol.* **430**, 20-26.

Tucker, D. K., Stahley, S. N. and Kowalczyk, A. P. (2014). Plakophilin-1 protects keratinocytes from pemphigus vulgaris IgG by forming calcium-independent desmosomes. *J. Invest. Dermatol.* **134**, 1033-1043.

Wolf, A., Keil, R., Götzl, O., Mun, A., Schwarze, K., Lederer, M., Hüttelmaier, S. and Hatzfeld, M. (2006). The armadillo protein p0071 regulates Rho signalling during cytokinesis. *Nat. Cell Biol.* **8**, 1432-1440.

Wolf, A., Krause-Gruszczynska, M., Birkenmeier, O., Ostareck-Lederer, A., Hüttelmaier, S. and Hatzfeld, M. (2010). Plakophilin 1 stimulates translation by promoting eIF4A1 activity. *J. Cell Biol.* **188**, 463-471.

Wolf, A., Rietscher, K., Glass, M., Huttelmaier, S., Schutkowski, M., Ihling, C., Sinz, A., Wingenfeld, A., Mun, A. and Hatzfeld, M. (2013). Insulin signaling via Akt2 switches plakophilin 1 function from stabilizing cell adhesion to promoting cell proliferation. *J. Cell Sci.* **126**, 1832-1844.